Biochimica et Biophysica Acta 1807 (2011) 746–754

Contents lists available at ScienceDirect

Biochimica et Biophysica Acta

journal homepage: www.elsevier.com/locate/bbabio

Carbon metabolism and the sign of control coefficients in metabolic adaptations underlying K-*ras* transformation ☆

Pedro de Atauri [a,1], Adrian Benito [a,1], Pedro Vizán [a,2], Miriam Zanuy [a], Ramón Mangues [b], Silvia Marín [a], Marta Cascante [a,*]

[a] Department of Biochemistry and Molecular Biology, University of Barcelona, (associated to CSIC, IBUB, IDIBAPS, XRQTC), 08028 Barcelona, Spain
[b] Oncogenesis and Antitumor Drug Group, Networking Research Center on Bioengineering, Biomaterials and Nanomedicine (CIBER-BBN) and Biomedical Research Institute Sant Pau (IIB-Sant Pau), Barcelona, Spain

ARTICLE INFO

Article history:
Received 15 July 2010
Received in revised form 29 November 2010
Accepted 30 November 2010
Available online 23 December 2010

Keywords:
Metabolic control analysis
Control coefficient signs
Carbon metabolism
K-Ras cell transformation

ABSTRACT

Metabolic adaptations are associated with changes in enzyme activities. These adaptations are characterized by patterns of positive and negative changes in metabolic fluxes and concentrations of intermediate metabolites. Knowledge of the mechanism and parameters governing enzyme kinetics is rarely available. However, the signs—increases or decreases—of many of these changes can be predicted using the signs of metabolic control coefficients. These signs require the only knowledge of the structure of the metabolic network and a limited qualitative knowledge of the regulatory dependences, which is widely available for carbon metabolism. Here, as a case study, we identified control coefficients with fixed signs in order to predict the pattern of changes in key enzyme activities which can explain the observed changes in fluxes and concentrations underlying the metabolic adaptations in oncogenic K-*ras* transformation in NIH-3T3 cells. The fixed signs of control coefficients indicate that metabolic changes following the oncogenic transformation—increased glycolysis and oxidative branch of the pentose-phosphate pathway, and decreased concentration in sugar-phosphates—could be associated with increases in activity for glucose-6-phosphate dehydrogenase, pyruvate kinase and lactate dehydrogenase, and decrease for transketolase. These predictions were validated experimentally by measuring specific activities. We conclude that predictions based on fixed signs of control coefficients are a very robust tool for the identification of changes in enzyme activities that can explain observed metabolic adaptations in carbon metabolism. This article is part of a Special Issue entitled: Bioenergetics of Cancer.

1. Introduction

Metabolic concentrations and fluxes are the constrained components characterizing the collective action of cell metabolism, which are modulated by enzymatic activities. However, we have partial knowledge of the components of cell metabolism and the constraints relating them. Specially, we have limited knowledge of the kinetic properties of the enzymes and their regulation. Moreover, the observed heterogeneity in cell populations, associated with phenomena like protein crowding, interactions between glycolytic enzymes, and reversible associations with structural proteins or organelles [1,2] should alter both components and constraints. These limitations are likely to make systems in part unpredictable, specifically the magnitude of the changes following alterations in the activity of enzymes. Interestingly, the predicted sign of changes in metabolite concentrations and metabolic fluxes following changes in enzyme activity is likely to be more robust and allows their prediction without requiring accurate kinetic information. Metabolic control analysis (MCA) [3–5] is one framework which permits the prediction of the signs of concentration and flux changes.

In the framework of MCA, systemic properties of the whole network are described as a function of the properties of enzymes isolated from the system. Steady state fluxes and metabolite concentrations are systemic properties. Enzyme rates, by contrast,

Abbreviations: ACoA, acetyl-CoA; Cit, citrate; DHAP, dihydroxyacetone-phosphate; E4P, erythrose-4-phosphate; F16BP, fructose-1,6-bisphosphate; F6P, fructose-6-phosphate; G6P, glucose-6-phosphate; G6PD, glucose-6-phosphate dehydrogenase; GAP, glyceraldehyde-3-phosphate; GAPDH, glyceraldehyde 3-phosphate dehydrogenase; HK, hexokinase; HexP, hexose phosphates; αKG, α-ketoglutarate; LDH, lactate dehydrogenase; Mal, malate; MCA, metabolic control analysis; Oaa, oxaloacetate; PenP, pentose phosphates; PPP, pentose-phosphate pathway; PEP, phosphoenol pyruvate; PFK, phosphofructokinase; Pyr, pyruvate; PK, pyruvate kinase; R5P, ribose-5-phosphate; S7P, sedoheptulose-7-phosphate; SucCoA, succinate-CoA; TKT, transketolase; TrisP, triose phosphates

☆ This article is part of a Special Issue entitled: Bioenergetics of Cancer.

* Corresponding author. Tel.: +34 4021593; fax: +34 4021559.
E-mail addresses: pde_atauri@ub.edu (P. de Atauri), adriabenito@ub.edu (A. Benito), Pedro.Vizan@cancer.org.uk (P. Vizán), mzanuy@ub.edu (M. Zanuy), rmangues@hsp.santpau.es (R. Mangues), silviamarin@ub.edu (S. Marín), martacascante@ub.edu (M. Cascante).

[1] These authors contributed equally to this work.

[2] Present address: Laboratory of Developmental Signalling, Cancer Research UK London Research Institute, London WC2A 3LY, United Kingdom.

0005-2728/$ – see front matter © 2010 Elsevier B.V. All rights reserved.
doi:10.1016/j.bbabio.2010.11.015

are properties of the isolated enzymes, and depend on the specific mechanism and parameters governing the enzyme kinetics. Under MCA, an *elasticity* ε_{qk} is the parameter sensitivity of the rate v_q of an isolated reaction—at steady state conditions—with respect to changes in the concentration x_k of one of its substrate, inhibitor or any other kinetic effectors of the isolated reaction [3,4]:

$$\varepsilon_{qk} = \frac{\partial \ln v_q}{\partial \ln x_k} \tag{1}$$

Similarly, a *control coefficient* is a system property defined as the sensitivity of a metabolite concentration x_g or a flux J_q with respect to changes in some parameter p—usually the enzyme concentration—which will in principle be proportional to the rate v_k when the enzyme is isolated, and then associated to the enzyme activity [3,4]:

$$C_{gk} = \frac{\partial \ln x_g}{\partial \ln p} \Big/ \frac{\partial \ln v_k}{\partial \ln p} = \frac{\partial \ln x_g}{\partial \ln v_k} \tag{2}$$

$$C_{qk} = \frac{\partial \ln J_q}{\partial \ln p} \Big/ \frac{\partial \ln v_k}{\partial \ln p} = \frac{\partial \ln J_q}{\partial \ln v_k} \tag{3}$$

Different approaches have been proposed for describing the control coefficients, including methods based on matrices [6–10] and those based on graph theoretical procedures [11,12]. These methods allow the derivation of large expressions describing the control coefficients, whose sign and magnitude are a function of the pathway stoichiometry, the elasticities, and the ratios of fluxes in branched pathways. In systems with moiety conservations, concentrations are also required [8,10]. The sign of a control coefficient—positive or negative—is sufficient to predict whether a flux or concentration will increase or decrease when an enzyme activity is changed. Positive control coefficient indicates that changes in x_g or J_q will follow the same pattern as changes in v_k. This means an increase of v_k will induce an increase of x_g or J_q, while decreasing v_k will also decrease the value of x_g or J_q. Negative control coefficient, on the contrary, indicates that changes in v_k will induce an inverse effect on the changes in x_g or J_q.

Some control coefficients have fixed signs, irrespective of the magnitudes of the elasticities and fluxes, and then they are either always positive or always negative [13,14]. Other control coefficients are sign-indeterminate, meaning they can be positive or negative, and some control coefficients are always zero. The classification into these types of control coefficients requires the only knowledge of the metabolic network structure and the direction of regulatory dependencies of the network, which basically refers to the positive or negative sign of the elasticities: i) elasticities with respect to substrates or activators are always positive; ii) elasticities with respect to inhibitors—or products in reversible reactions—are always negative. The fixed sign will be maintained while both structure and qualitative regulatory dependencies are maintained. Each control coefficient predicts changes in fluxes and concentrations resulting from the change of one enzyme activity. In general, the predictive value of this normalized derivative is accurate for infinitesimal changes of the enzyme activity and decays for larger changes due to the redistribution of the elasticities and fluxes. The prediction of the sign of a sign-fixed control coefficient is a positive or negative direction that is not modified for large changes.

In the present work, we take advantage of sign-fixed control coefficients to derive hypotheses about the enzyme activities which are modified in order to achieve specific changes in glycolytic and pentose phosphate pathway (PPP) fluxes and concentrations. As a case study of metabolic reprogramming, we have analyzed the transformation with mutated *K-ras* oncogenes of a mouse embryonic fibroblast cell line NIH-3T3. Oncogenic Ras-transformed NIH-3T3 cells have been used as a model system to explore characteristics associated with cell transformation, such as a higher aerobic glycolysis and changes of enzyme activities [15–18]. Ras proteins are a family of small GTPases activated in response to extracellular stimuli and leading to the activation of several signalling cascades [19–21]. Among the different isoforms, K-Ras is the Ras protein which plays a major role in cancer. NIH-3T3 cells stably transfected with constitutively active K-*ras* mutated at codon 12 or codon 13 (K12- and K13-transformed cells) induce tumours with distinct survival strategies, associated with distinct transforming capabilities and aggressiveness [22,23]. Previously, we measured significant changes in carbon metabolism of K12- and K13-transformed cells based on stable-isotope (^{13}C) tracer-based technologies [24]. Interestingly, both mutants showed an increased utilization of the oxidative branch of the PPP, higher for K13 cells, compared with non-transformed NIH-3T3 cells.

In order to derive hypotheses about the enzyme activities that contribute to the reprogramming of carbon metabolism: 1) we characterized metabolic adaptations in non-transformed and K12- and K13-transformed cells by means of experimentally measured external and internal metabolite concentrations; and 2) we computed the network flux distribution using a constraint based approach and the data obtained of external metabolite variations; 3) we identified control coefficients with fixed signs in order to predict the pattern of changes in enzyme activities which can explain the observed increases or decreases in fluxes and concentrations; and 4) finally, we measured specific activities of key enzymes in order to validate the predictions on the enzyme activity increases or decreases compatible with the observed flux and concentration changes.

2. Materials and methods

A combination of experimental and mathematical–computational methods was applied including the measurement of glucose uptake (J_A), lactate production (J_T), and glutamate–glutamine uptake (J_U) together with measurements of sugar phosphate concentrations and enzyme specific activities. All measures were replicated in independent experiments. Mathematical–computational methods were performed using *Mathematica* [25].

2.1. Cell lines and culture

NIH-3T3 cells were obtained from the American Type Cell Culture (ATCC). The transfectants contained a K-*ras* minigene with a G:C → A:T mutation at the first position of codon 12 (K12 cells) and a G:C → A:T mutation at the second position of codon 13 (K13). All lines were maintained in Dulbecco's Modified Eagle Medium (DMEM) in the presence of 10% FBS, 25 mM D-glucose and 4 mM L-glutamine, at 37 °C in 95% air–5% CO_2. Geneticin© Selective Antibiotic (GIBCO) was used as a selective antibiotic in K12 and K13 cells.

For biochemical and enzyme activity measurements, cells were seeded in p100 dishes at different densities between $0.8 \cdot 10^6$ and $1.2 \cdot 10^6$ cells/cm^2. 24 h after seeding, incubation medium was removed and cells were incubated for 72 h with DMEM containing 10% FBS, 25 mM D-glucose and 4 mM L-glutamine. At the end of the incubations, media for biochemical analysis were removed and frozen at −20 °C until processing. Cells for sugar phosphates determination were immediately frozen in liquid nitrogen and kept at −80 °C until processing. Cells for activity measurements were washed with PBS and scrapped in a lysis buffer as detailed below. Cell counting was performed with a haemocytometer.

2.2. Protein concentration

Protein concentration of cell extracts was determined using the BCA Protein Assay (Pierce Biotechnology, Rockford, IL).

2.3. Measurements of media metabolites consumption and production

Glucose, lactate, glutamate, and glutamine concentrations were determined from frozen medium samples as previously described [26–28] using a Cobas Mira Plus chemistry analyzer (ABX). The rates of the medium metabolites consumption/production—glucose consumption (J_A), lactate production (J_T) and glutamate from glutamine consumption (J_U)—are derived from the total measured consumptions/production of metabolites and corrected according to the measured cell proliferation, assuming exponential growth and constant consumption or production. The rate of glutamate from glutamine consumption is derived from the measured rates of glutamine consumption and glutamate accumulation. All the values are expressed in micromol of metabolite consumed or produced per milligram of protein and hour (μmol mg prot^{-1} h^{-1}).

2.4. Sugar phosphates determination

Hexose, pentose and triose phosphates were determined in cell monolayers frozen in liquid nitrogen using addition curve methods as described [29]. The MRM (multiple reaction monitoring) transitions were 339/97 for fructose-1,6-bisphosphate (F16BP), 259/97 for glucose-6-phosphate (G6P) and fructose-6-phosphate (F6P) (hexose phosphates) (HexP), 229/97 for ribose-5-phosphate (R5P) and xylulose-5-phosphate (pentose-phosphates) (PenP), 169/97 for glyceraldehyde-3-phosphate (GAP) and dihydroxyacetone phosphate (triose phosphates) (TrisP) and 167/79 for phosphoenol pyruvate (PEP). Sugar phosphate concentrations are expressed as nanomol per milligram of protein (nmol mg prot^{-1}).

2.5. Enzyme activity determinations

Activities of the glycolytic enzymes hexokinase (HK), pyruvate kinase (PK), and lactate dehydrogenase (LDH), and PPP enzymes glucose-6-phosphate dehydrogenase (G6PD) and transketolase (TKT), were determined from cell culture extracts. Enzyme activities are expressed as milliunits per milligram of protein (mU mg prot^{-1}).

Preparation of cell extracts for enzyme activity determination. Cell cultures were washed with PBS and scrapped in lysis buffer (20 mM Tris–HCl, pH 7.5, 1 mM dithiothreitol, 1 mM EDTA, 0.02% Triton X-100, 0.02% sodium deoxycholate) supplemented with protease and phosphatase inhibition cocktails. Cell lysates were disrupted by sonication (3 cycles of 5 s) and immediately ultracentrifuged at 105,000 ×*g* for 1 h at 4 °C. The supernatant was separated and used for the determination of enzyme activities using a Cobas Mira Plus chemistry analyzer (HORIBA ABX, Montpellier, France). All enzymatic activities were determined by monitoring NADH/NADPH increment or decrement at a wavelength of 340 nm.

A strong decrease of the mitochondrial Complex I activity has been recently reported in K-*ras* transformed cells [30]. The conditions of extract preparation using a soft lysis buffer as well as soft sonication have been optimised to minimise the extraction of mitochondrial Complex I activity and other membrane-bound enzymes. The absence of unspecific coenzyme (NADH or NADPH) consumption/production has been checked before the addition of the reaction substrate for all the enzyme activities measured.

Glucose-6-phosphate dehydrogenase (G6PD, EC 1.1.1.49) activity was measured as described in Tian et al. [31]. Briefly, samples were added to a cuvette containing 0.5 mM $NADP^+$ in 50 mM Tris–HCl, pH 7.6 at 37 °C. Reactions were initiated by the addition of G6P up to a final concentration of 2 mM.

Hexokinase (HK, EC 2.7.1.1) activity was determined by coupling HK reaction to G6PD enzyme in the following conditions: 3.3 mM $NADP^+$, 14.8 mM ATP, 14.8 mM $MgCl_2$, 2.8 U/mL G6PD and 50 mM Tris–HCl, pH 7.6 at 37 °C. Reactions were initiated by the addition of glucose to a final concentration of 10 mM.

Transketolase (TKT, EC 2.2.1.1) activity was determined using the enzyme linked method described by Smeets and colleagues [32]. Briefly, samples were added to a cuvette containing 5 mM $MgCl_2$, 0.2 U/ml triose phosphate isomerase, 0.2 mM NADH, 0.1 mM thiamine pyrophosphate in 50 mM Tris–HCl, and pH 7.6 at 37 °C. The reaction was initiated by the addition of a substrate mixture in 1:2 proportion (substrate mixture : final volume) prepared by dissolving 50 mM R5P in 50 mM Tris–HCl, pH 7.6 with 0.1 U/ml ribulose-5-phosphate-3-epimerase and 1.7 mU/ml phosphoriboisomerase. The substrate mixture was continuously stirred and heated for 1 h at 37 °C and then kept at −20 °C until use.

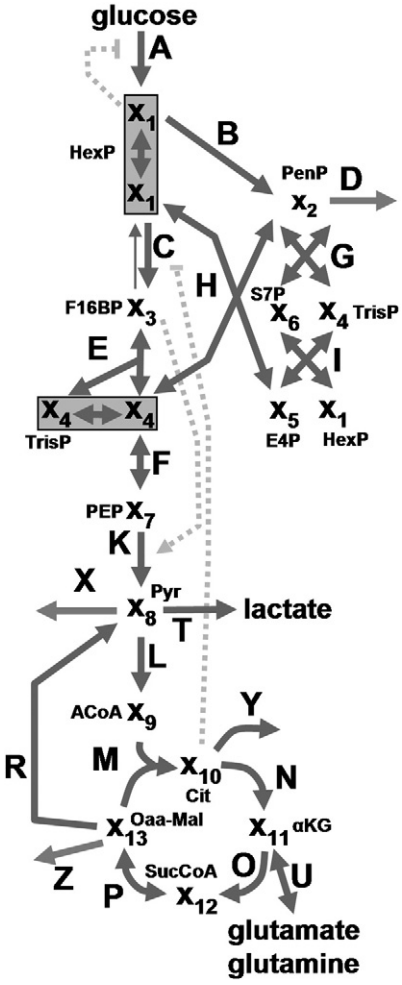

Fig. 1. Network scheme. Each arrow indicates a reversible or irreversible reaction step catalyzed by an enzyme (or transporter) or one block of enzymes. Grey dashed lines account for the regulatory circuits (inhibitions and activations).

Pyruvate kinase (PK, EC 2.7.1.40) activity was determined by coupling the PK reaction to the LDH enzyme in the following conditions: 0.8 mM NADH, 1.6 mM ADP, 12.1 mM $MgCl_2$, 36.8 mM KCl, 5.2 U/mL LDH in 20 mM phosphate buffer, pH 7.2 at 37 °C. Reactions were initiated by the addition of PEP up to a final concentration of 3.5 mM.

Lactate Dehydrogenase (LDH, EC 1.1.1.27) activity was measured at 37 °C by adding sample extracts to a cuvette containing 0.2 mM of NADH and 100 mM phosphate buffer, pH 7.4. Reaction was initiated by the addition of pyruvate (Pyr) up to a final concentration of 0.2 mM.

2.6. Isotopomer abundances

^{13}C labelled substrates generate for each metabolic product a set of different labelled molecules—*isotopomers*—that differ only in the labelling state of their individual carbon atoms. In a previous paper [24] 50% [1,2-^{13}C]-D-glucose was used as tracer and the generation of ^{13}C labeled products was measured retaining for each product the relative abundances of the non-labelled isotopomer form (m0), and

the isotopomers with one ^{13}C (m1), two ^{13}C (m2), three ^{13}C (m3), etc. The isotopomer abundances of lactate are here applied to describe the ratio of fluxes through oxidative PPP (J_B) with respect to the entry of glucose (J_A) [33]: $f1 = J_B/J_A = 3\times(m1/m2)/(3+(m1/m2))$.

2.7. Statistical analysis

Two-tailed Student's t-test was performed in order to compare metabolite concentrations and activities of non-transfected against K12- and K13-transfected cells. Differences were considered significant for $p<0.1$.

3. Results

3.1. Metabolic adaptations in K12- and K13-transformed NIH-3T3 cells

3.1.1. System description

The scheme of the whole network under study is depicted in Fig. 1. Fluxes are represented with letter *J*, where J_i refers to the steady state metabolic flux through the *i*th step; concentrations are represented with letter *x*, where x_i refers to the concentration of the *i*th metabolic intermediary; and activities are represented with letter *v*, where v_i refers to the rate of the isolated reaction of the *i*th step. Solid arrows (Fig. 1)—reaction steps *A* to *Z*—refer to the principal carbon metabolism, including glycolysis, the PPP, the tricarboxylic acid cycle and the main inputs and outputs. Some reactions were neglected and grouped into blocks—e.g. reaction step *F* refers to the block from glyceraldehyde 3-phosphate dehydrogenase (GAPDH) to enolase—and others were assumed to be involved in rapid equilibriums—e.g. glucose-6-phosphate isomerase. Metabolites were combined into different pools: the pool x_1 for HexP refers to G6P and F6P; the pool x_2 for PenP refers to R5P; ribulose-5-phosphate and xylulose-5-phosphate; the pool x_4 for TrisP refers to dihydroxyacetone-phosphate (DHAP) and GAP; and the pool x_{13} refers to oxaloacetate (Oaa) and malate (Mal). The rest of metabolic intermediaries are F16BP (x_3), sedoheptulose-7-phosphate (x_6; S7P), erythrose-4-phosphate (x_5; E4P), PEP (x_7), Pyr (x_8), acetyl-CoA (x_9; ACoA), citrate (x_{10}; Cit), α-ketoglutarate (x_{11}; αKG) and succinate-CoA (x_{12}; SucCoA). In our system, the main fluxes in or out of the defined metabolic network correspond to experimentally measured glucose consumption (J_A), glutamate from glutamine consumption (J_U), and lactate production (J_T). Additional output exchanges connected to biosynthetic processes were not associated with a measured value (J_D, J_X, J_Y, J_Z).

3.1.2. Flux distributions

Under steady-state conditions, the flux balance associated with the stoichiometry constrains the dependences among fluxes [34–36]. In order to estimate the different flux distributions of non-transformed, K12- and K13-transformed cells, the fluxes for internal reactions can be expressed as dependent on a subset of fluxes including all output and input fluxes, e.g.:

$$\begin{aligned}
J_C &= J_E = J_A - {}^1/_3\,(J_B + 2\times J_D),\\
J_F &= J_K = 2\times J_A - {}^1/_3\,(J_B + 5\times J_D),\\
J_{Gf} &= {}^1/_3(J_B - J_D) + J_{Gb},\\
J_{Hf} &= {}^1/_3\,(J_B - J_D) + J_{Hb},\\
J_{If} &= {}^1/_3\,(J_B - J_D) + J_{Ib},\\
J_L &= J_M = 2\times J_A - {}^1/_3\,(J_B + 5\times J_D) - J_T + J_U - J_X - J_Y - J_Z,\\
J_N &= 2\times J_A - {}^1/_3(J_B + 5\times J_D) - J_T + J_U - J_X - 2\times J_Y - J_Z,\\
J_O &= J_P = 2\times J_A - {}^1/_3\,(J_B + 5\times J_D) - J_T + 2\times J_U - J_X - 2\times J_Y - J_Z,\\
J_R &= J_U - J_Y - J_Z,
\end{aligned} \tag{4}$$

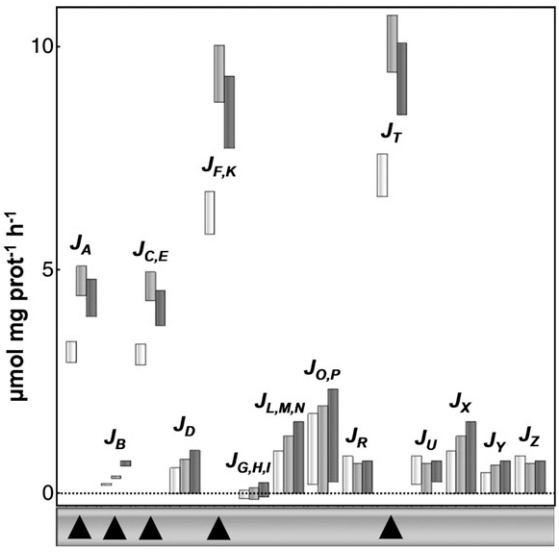

Fig. 2. Comparison of fluxes. Non-transformed NIH-3T3 cells (white); K12-transformed cells (light gray); and K13-transformed cells (dark gray). ▲) Increased flux in transformed cells with respect to non-transformed cells; and ▼) Decreased flux in transformed cells with respect to non-transformed cells. Some dependent fluxes are grouped together: J_C *and* J_E ($J_{C,E}$); J_F *and* J_K ($J_{F,K}$); J_G, J_H *and* J_I ($J_{G,H,I}$) ; J_L, J_M *and* J_N ($J_{L,M,N}$); *and* J_O *and* J_P ($J_{O,P}$).

where J_{Gf}, J_{Hf}, J_{If} and J_{Gb}, J_{Hb}, J_{Ib} are the forward (J_{if}) and backward (J_{ib}) fluxes through the reversible reactions $J_G = J_{Gf} - J_{Gb}$, $J_H = J_{Hf} - J_{Hb}$, and $J_I = J_{If} - J_{Ib}$. An additional constraint was imposed based in our previous isotopomer-based analysis of non-transformed NIH-3T3 cells and K12- and K13-transformed cells [24] (see Section 2.6):

$$J_B = f_1 \times J_A \tag{5}$$

where factor f_1 relates the oxidative branch of PPP (J_B) with the entry of glucose (J_A). This factor was set according to the measured ratios [24]: 0.063 ± 0.004 for non-transformed cells; 0.076 ± 0.012 for K12-transformed cells; and 0.153 ± 0.016 for K13-transformed cells. Thus, the flux through the oxidative branch of PPP was significantly lower than that descending through the glycolysis, and there was a significant increase of the flux through the PPP in transformed cells compared to non-transformed NIH-3T3 cells. Between transformed cells, K13 mutants routed more glucose to the oxidative branch of PPP than K12 mutants.

All these assumptions and measures are constraints limiting the space of solutions for the internal metabolic fluxes. Unfortunately, the complete system cannot be determined with the available measurements. Uncertainty is associated with the measured exchange fluxes (J_A, J_T, J_U) and, specially, with those not measured (J_X, J_Y, J_Z, J_D). An interval constraint satisfaction approach was applied as suggested by Llaneras and Picó [37] for cases where available measurements are insufficient and the complete flux distribution cannot be uniquely calculated. The feasible range of solutions satisfying all constraints was estimated for each reaction step. Initial lower and upper bounds for intervals were assigned to the flux through all reaction steps: 1) lower and upper bounds were assigned as the mean value ± 1.5 × standard deviation for measured fluxes J_A, J_T, and J_U; 2) a lower bound of zero was assumed for the irreversible fluxes $J_B, J_D, J_K, J_L, J_M, J_N, J_O, J_R, J_S, J_X, J_Y, J_Z$, which were assumed to have positive values ($0 < J_i$). For each cell type, the lower and upper bounds were constrained to satisfy the stoichiometric description of the system Eq. (4) and the isotopomer-based constraint in Eq. (5). These intervals of fluxes satisfying all constraints were calculated by two independent procedures: 1) iterative interval propagation, or 2) solving each minimum and maximum bound through linear programming, taking

advantage of the linear nature of the problem. The resulting flux distributions for non-transformed cells, K12- and K13-transformed cells are shown in Fig. 2, which graphically depicts the interval ranges of flux values which satisfy all the constraints. As an example, for non-transformed cells, the initial intervals were $2.04<J_A<3.41$, $0<J_B<\infty$, $-\infty<J_C<\infty$, $0<J_D<\infty$, $-\infty<J_E<\infty$, $-\infty<J_F<\infty$, $0<J_G<\infty$, ..., $6.63<J_T<9.56$, $0.20<J_U<0.84$,..., and the final intervals satisfying all constraints (solution space) computed with both iterative interval propagation and linear programming were $2.93<J_A<3.41$, $0.18<J_B<0.21$, $2.86<J_C<3.34$, $0<J_D<0.57$, $2.86<J_E<3.34$, $5.80<J_F<6.75$, $-0.11<J_G<0.07$, ..., $6.63<J_T<7.59$, $0.20<J_U<0.84$, ... Even with the propagated uncertainty, substantial changes in flux distribution are detected in transformed cells with respect non-transformed cells, in particular for the flux pattern in glycolysis and the oxidative branch of the PPP.

3.1.3. Metabolite concentrations

Changes in fluxes were coupled with additional experimental measurement of key sugar phosphate concentrations. Thus, the concentrations of HexP (x_1), PenP (x_2), F16BP (x_3), TrisP (x_4), and PEP (x_7) were measured for non-transformed and transformed cells (K12 and K13) and are compared in Fig. 3. All concentrations were found to be slightly decreased in transformed cells.

3.2. Predicted changes in fluxes and concentrations

3.2.1. The sign of control coefficients

In order to identify control coefficients with fixed signs, all regulatory dependences were considered. The matrix approach proposed by Cascante et al. [9,10] was applied and is depicted in Fig. 4. A matrix M^{-1} with all concentration control coefficients and all independent flux control coefficients can be derived from the inverse of a matrix M containing all elasticities and flux dependences. The sign of the elasticities is taken in order to derive the sign of the control coefficients. For example, the dependence of G6PD (reaction step B) on its substrate (HexP, x_1) corresponds to a positive elasticity ε_{B1}. In Fig. 1, grey dashed lines account for the regulatory circuits—i.e. product (G6P, x_1) inhibition of HK (reaction step A) [38], inhibition of phosphofructokinase (PFK, reaction step C) by Cit (x_{10}) [39] and activation of PK (reaction step K) by F16BP (x_3) [40,41], which are associated with negative (ε_{A1}), negative (ε_{C10}) and positive (ε_{K3})

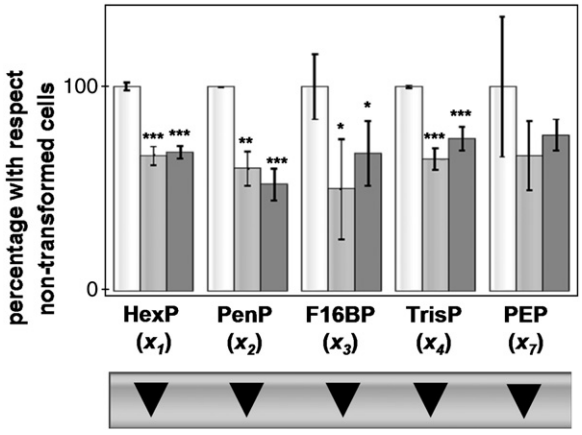

Fig. 3. Comparison of measured concentrations. Values for concentrations are proportional to the bar height for each chemical specie and error bars correspond to standard deviations. See legend of Fig. 2 for meaning of colours and triangles. As a reference for sugar phosphate concentrations, [F16BP] = 3.229 nmol mg prot^{-1}, [HexP] = 1.799 nmol mg prot^{-1}, [PenP] = 0.726 nmol mg prot^{-1}, [TrisP] = 2.710 nmol mg prot^{-1} and [PEP] = 0.457 nmol mg prot^{-1} for non-transformed NIH-3T3 cells. P-values using two-tailed Student's t-test: *: $p<0.1$, **: $p<0.05$; ***: $p<0.01$.

elasticities, respectively. Reversibility is associated with negative elasticities with respect to products. Finally, reaction steps D, X, Y and Z describing the demand of synthetic processes were assumed to be saturated with respect to their respective substrates and then controlled by the demand; so, the elasticities ε_{D2}, ε_{X8}, ε_{Y10}, and ε_{Z13} were set to be zero.

The sign of each control coefficient was analyzed by checking the positivity or negativity of the determinant $|M|$ and the adjoint matrices in $Adj(M)$ used for the derivation of the inverse:

$$M^{-1} = \frac{1}{|M|}(Adj(M))^{\mathrm{T}} \tag{6}$$

Since the determinant |M| was positive, the sign depended on the adjoint matrices. The matrix M^{-1} in Fig. 4b shows all control coefficients for independent fluxes and concentrations derived from this analysis. Control coefficients for the dependent fluxes can be derived by considering the dependences among fluxes in Eq. (4) and the control coefficients of independent fluxes [9,10], as demonstrated in the example provided in Fig. 4c. A subset of control coefficients signs are presented in Fig. 4d in a table of dependences between the fluxes and concentrations and the main enzyme activities. Positive and negative symbols correspond to control coefficients with positive and negative signs, respectively. The signs in Fig. 4d collectively give a complete systemic predictive tool which can be used to evaluate the expected impact of changes in enzyme activities. Thus, the specific pattern of observed changes in fluxes and concentrations can be associated with increases or decreases of enzyme activities through analysis of the signs of control coefficients. For example, the observed decrease in the concentration of PEP (x_7) could correspond to an increase of PK activity (v_K), but never due to a decrease.

3.2.2. The magnitude of the control coefficients

The analysis of the signs of metabolic control coefficients is sufficient if the aim is to predict the direction of changes in concentrations and fluxes. However, this previous analysis does not suffice if the objectives are to predict the magnitudes of these changes, and then the magnitude of the control coefficients is required. Unknown elasticities can be randomly sampled in order to derive feasible magnitudes for control coefficients [42]. We have applied sampling procedures based on those described by Wang et al. [42] in order to have an additional independent evaluation of the sign and mean magnitude of the control coefficients (results exactly match the computed signs). This analysis identified a subset of control coefficients which are always associated with small magnitudes. In the system considered (Fig. 1) the PPP is a sub-network characterized by a flux which is much smaller than the main fluxes through the rest of the network ($J_B \lll J_C$). The effect of changes in the activity throughout this sub-network will have minimal effect on the rest of the system, but these changes can have a significant effect on the concentrations and reaction steps inside the sub-network. The dependence of control coefficients on particular fluxes, such as J_B, can be easily identified by inspecting the adjoint matrices. Control coefficients identified with black circles in Fig. 4d are directly proportional to the value of J_B, which implies very small magnitudes due to the small flux through the oxidative branch of the PPP.

3.3. Testing and validation of hypotheses based on variations in enzyme activities

3.3.1. Specific activities

The specific activities of HK (v_A), G6PD (v_B), TKT (v_G, v_H), PK (v_K), and LDH (v_T) were measured for non-transformed and transformed (K12 and K13) cells and compared in Fig. 5a. Increases or decreases in specific activities observed during the metabolic adaptation associated with the K-*ras* transformation were analysed. Clear changes were observed for

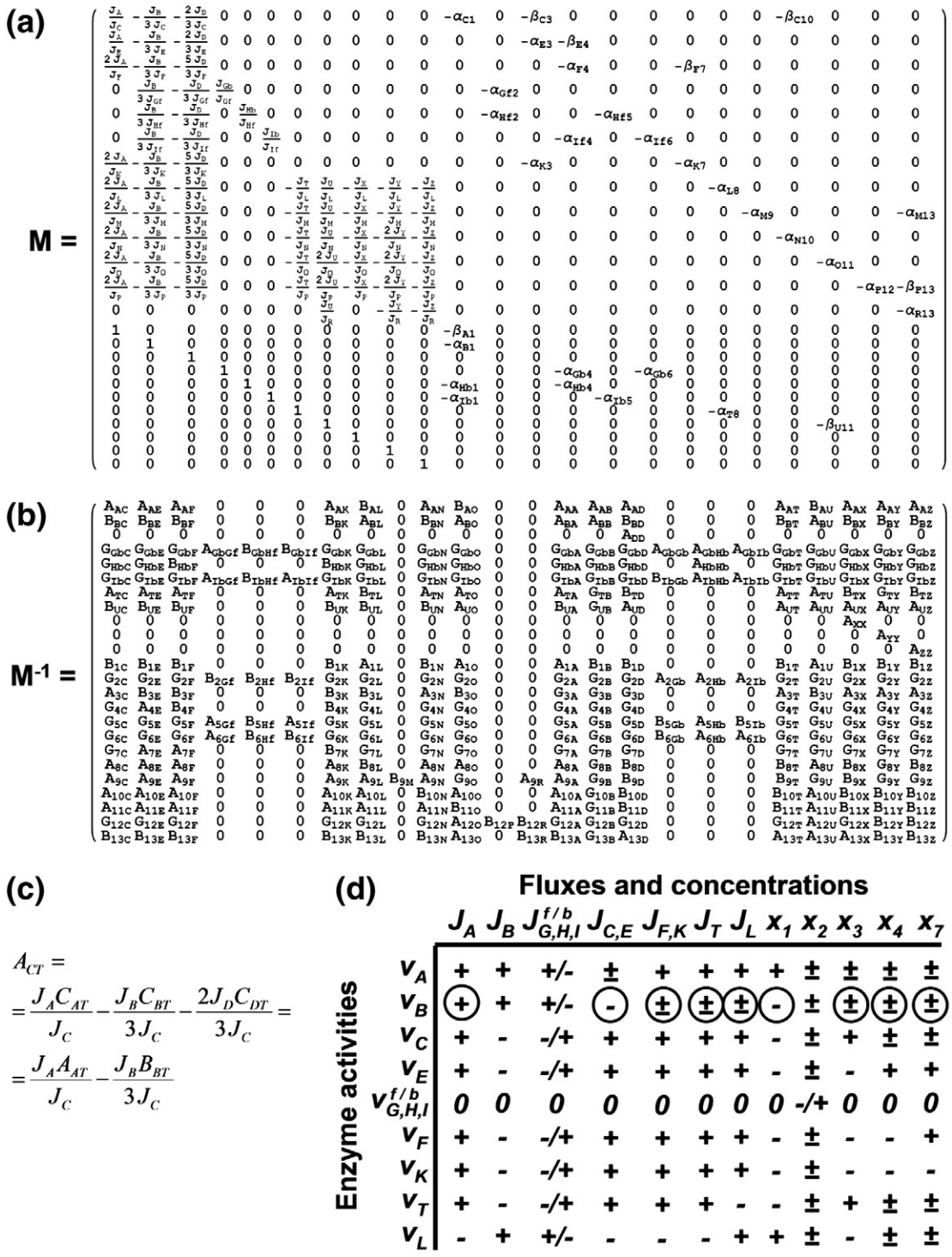

Fig. 4. Matrix estimation of the sign of control coefficients. For details about the method see [9,10]. Elasticities with a magnitude of zero appear as *0*, while those positives are represented with a letter α ($\alpha_{ki}=\varepsilon_{ki}>0$), and those negatives with a letter β ($\beta_{ki}=\varepsilon_{ki}<0$); control coefficients with a magnitude of zero appear as *0*, while these positives are represented with the letter *A* ($A_{ki}=C_{ki}>0$) or a symbol "+", and these negatives with the letter *B* ($B_{ki}=C_{ki}<0$) or a symbol "−"; Those control coefficients with indeterminate signs are represented with a letter *G* ($G_{ki}=C_{ki}>0$ *or* $C_{ki}<0$) or a symbol "±". A matrix *M* (a) with the information containing both the stoichiometry and the regulatory properties of the analysed system (elasticities and ratios among fluxes), is inverted to obtain the matrix of control coefficients M^{-1} (b) for independent fluxes and concentrations. (c) An example of estimation of a control coefficient of dependent fluxes from the previously estimated control coefficients of independent fluxes. (d) Table of dependences connecting changes in fluxes and concentrations with changes in enzyme activities for a subset of analyzed control coefficients. Superscripts "f" and "b" refers to net direction of reversible reactions of the non-oxidative branch of PPP (*G,H,I*) following the forward or the backward directions, respectively. The net fluxes for the remaining reversible reactions are set to follow only the forward direction according to Fig. 2. Symbols ("+","−","±") identified with a black circle refer to control coefficients of very low magnitude in comparison with the other ones (see Section 3.2.2).

G6PD and LDH for both K12 and K13 transformed cells, with slight changes also for TKT with both K12 and K13 transformed cells and also for PK with K13 transformed cells. There were no significant changes in the observed HK activities.

3.3.2. Do changes in measured activities satisfy the predictions for concentrations and fluxes?

The table of dependences in Fig. 5b identifies both satisfied and non-satisfied predictions of the sign of control coefficients for those

activities with measured changes (v_B, v_G, v_H, v_K and v_T). Satisfied predictions, which are those where the direction of the changes in a concentration or flux is explained by the direction of the change in an enzyme activity, are marked in green. Otherwise, if the prediction is not satisfied, the sign of the control coefficients is marked in red. For example, the increase in LDH activity (v_T) could help to explain the measured increase in J_A, but not the increase in J_B, which is satisfied by the increased G6PD activity (v_B). Predictions regarding TKT are more complicated because the slight decrease of TKT activity could contribute to a predicted decrease of PenP levels (x_2), but only if the net flux through the non-oxidative branch of PPP is following the backward direction to PenP as is shown in Fig. 5b.

Indeterminate signs (±) identify control coefficients that can be positive or negative, depending on the relative values of the elasticities and ratios between fluxes. For a set of such sign-indeterminate control coefficients, only a limited combination of positive and negative signs is possible. Indeterminate signs (±) marked in green were used in Fig. 5b to highlight that a specific and feasible combination of elasticities and fluxes can result in a combination of signs which satisfy the changes in fluxes and concentrations. For example, the measured decreases in x_2, x_4, and x_7 can be predicted by an increase in v_T activity, which is possible because the negative control coefficients for C_{2T}, C_{4T}, and C_{7T} can be obtained by selecting the appropriate elasticities.

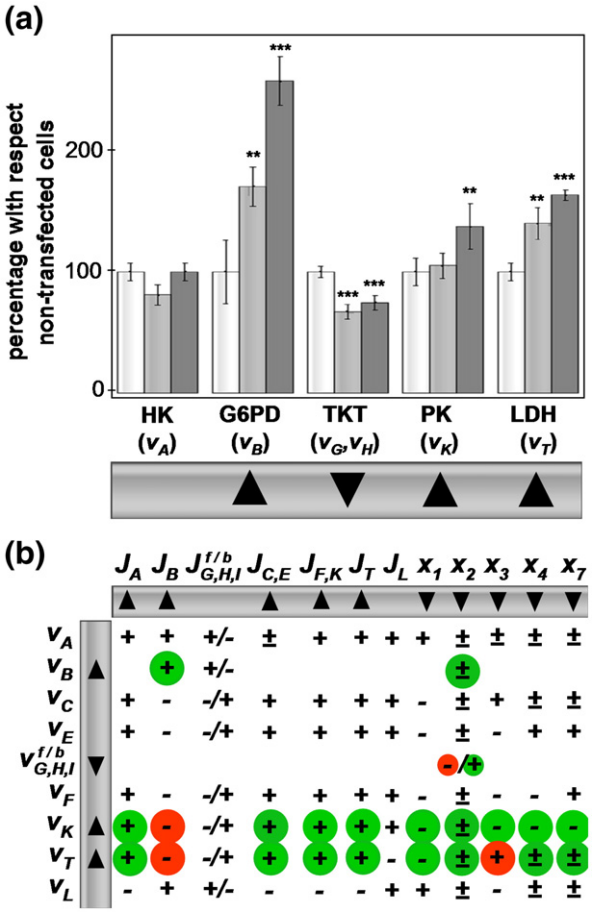

Fig. 5. Specific activities and satisfied predictions. (a) Comparison of specific activities. See legend of Figs. 2 and 3 for meaning of bar height, error bars, colours and triangles. As a reference for specific activities, HK = 130.17 mU mg prot^{-1}, LDH = 2.83 U mg prot^{-1}, G6PD = 215.02 mU mg prot^{-1}, TKT = 35.72 mU mg prot^{-1} and PK = 6.98 U mg prot^{-1} for non-transformed NIH-3T3 cells. P-values using two-tailed Student's t-test: *: $p<0.1$, **: $p<0.05$; ***: $p<0.01$. (b) Satisfied predictions represented in the table of dependences connecting changes in fluxes and concentrations with changes in enzyme activities. See legend of Fig. 4 for meaning of superscripts "f" and "b", and positive-negative symbols ("+","−","±"). Symbols marked in green or red refers to control coefficients that can explain or cannot explain, respectively, the observed directions of a change in a flux or a concentration with respect to the direction of a measured change in an enzyme activity (see Section 3.3.2).

4. Discussion

The existence of control coefficients with fixed or indeterminate signs is dependent on the topology of the metabolic pathway and location of regulatory loops (feedback, feed-forward), branches, etc. [13]. The signs of the control coefficients estimated above (Fig. 4) were obtained by assuming a model adapted to the available data, where the relevant topology and regulation are considered. Analysis of the signs of control coefficients in Fig. 5b provides a complete picture of the potential effect that any change in enzyme activities would have on systemic properties such as fluxes and metabolite concentrations. This picture confirms that the increased fluxes from glucose to lactate (J_A, J_C, J_E, J_F, J_K, J_T) and through the oxidative part of the PPP (J_B) (Fig. 2), and the decreased concentrations of sugar phosphates (x_1, x_2, x_3, x_4, x_7) (Fig. 3), observed in transformed cells, can be explained in part by the increased specific activities for G6PD (v_B), PK (v_K), LDH (v_T), and decreased activity of TKT (v_G,v_H) (Fig. 5a). Interestingly, the differences between the phenotypes of K12 and K13 tranformed cells [22–24] are reflected by the magnitude of the changes in fluxes and not by the sign of these changes. Changes in enzyme activities are also in the same direction (with the same sign of change) for both transformed cells with the exception of PK activity which is only increased significantly in the K13 cell line.

The measured changes in specific enzyme activities accounts for changes in the enzyme concentrations. It should be noted that *in vivo*, changes affecting an enzyme activity can be as a result of the changes on its expression but also due to a variety of events including: changes in cofactors, post-transductional modification or changes in oligomerization state among others. One example of this is the case of PK. Among the different PK isoforms, the M2-PK isoenzyme is expressed in all proliferating cells, including embryonic, tumour and NIH-3T3 cells [41]. The M2-PK isoenzyme occurs in a highly active tetrameric form and in a dimeric form with low affinity for PEP [40]. The tetramer to dimer ratio of M2-PK is not static and depends on F16BP levels in addition to any effects due to other external mechanisms [40].

The measured changes of the specific activities for G6PD (v_B), PK (v_K), and LDH (v_T) satisfy the predictions based on the sign of the control coefficients. Interestingly, Fig. 5b shows that the set of observed changes in fluxes and concentrations accompanying K12- and K13-transformation cannot be attributed to the perturbation of a single enzyme activity. According to results depicted in Fig. 5b, simultaneous activation of G6PD and some of the glycolytic enzymes is required in order to fully explain the observed pattern of changes in fluxes and metabolite concentrations. The experimentally measured increase in G6PD and in some glycolytic enzymes (LDH (v_T) and PK (v_K)) confirms this prediction and helps to explain qualitatively almost all observed increases in fluxes and decreases in concentrations, although it is likely that other glycolytic enzyme activities could also be increased. The predictions of Fig. 5b are also in agreement with the available literature on tumour metabolism that suggests the action of transcription factors, as c-myc and the hypoxia-inducible transcription factor 1 (HIF-1), which are associated with the activation of oncogenes including transforming *ras*. This leads to the reprogramming of different components of the cell metabolism, including higher expression for most of the genes encoding glycolytic enzymes [38,43–48]. Among the enhanced enzymes are mammalian isoforms of HK (HK1 and 2), PK (M2-PK) and LDH (LDH-A). We have also observed changes in LDH for both K12 and K13 cells in addition to changes in PK for K13 cells. However, HK activity is not significantly altered by either of the two transformed cell

lines. Interestingly, in the previous work of Guerrero et al. [22,23] for the same K12- and K13-transformed NIH-3T3 cells used in the present study, they showed an increased expression of GAPDH for both transformed cell lines with respect to the non-transformed ones. From Fig. 5b we can predict that this increase of GAPDH (v_F) can also contribute to the observed metabolic phenotype of transformed cells.

Taking into account that control is distributed among the enzymes of glycolysis, it is not surprising that simultaneously increasing a number of different glycolytic enzymes is required in order to achieve a large increase in glycolytic flux. Thus, in a linear pathway, all the control coefficients are positive and their sum is equal to one [3], which means that, if the control is shared between several enzymes, then the magnitude of each individual control coefficient is expected to be quite low. A very low control coefficient indicates that in order to alter the flux significantly by using modifications of a single enzyme, a very large change in the enzyme concentration is required. However, a simultaneously balanced change in all glycolytic enzyme concentrations should result in both a directly proportional change in the glycolytic flux and also the absence of change in intermediate metabolites [49]. The observed slight decrease in all measured metabolites could be the consequence of increased external demands.

However, it is also interesting to notice that according to Fig. 5b the observed increase in the flux through the oxidative part of PPP is not predicted by an increase in measured glycolytic activities, but is clearly satisfied by an increase in G6PD activity. Comparing K12 and K13 cells, there is a perfect agreement between the higher G6PD activity and the higher flux through the oxidative part of the PPP. Regulation of the expression of G6PD is altered in many tumours, resulting in a significant increase in G6PD activity, and it has been suggested that G6PD may act as a potential oncogene [50]. Increased G6PD activity in NIH-3T3 cells, transfected with human G6PD cDNA, leads to tumorogenic transformations, dividing more quickly and inducing tumors in nude mice [50]. The decreased levels of PenP (x_2) are not compatible with the increased activity of G6PD, but are compatible with an increased demand of ribose (reaction step D). Also, the decreased levels of PenP can be at least in part a consequence of the slight decrease in the TKT activity. The two key enzymes of the PPP, G6PD and TKT, were both previously identified as potential targets in cancer therapy [51–54], and recently, the increased G6PD/TKT ratio was proposed as a tumour metabolome feature [55]. The observed notorious increase of G6PD resulted in a higher G6PD/TKT ratio in both transformed cell lines with respect to non-transformed cells in agreement with the results of Montoya et al. [55]. Here, we have also found that this ratio is higher in K13 than in K12.

Finally, it is interesting to note the fact that metabolic adaptations observed in transformed cells require changes in more than one enzyme, which suggests that a multi-hit strategy would be required to counteract metabolic adaptations in transformed cells. These results support the suggestions of Moreno-Sanchez et al. [56] who proposed that a "multi-targeted MCA advised therapy" would be required to design efficient treatments in cancer based on the fact that control is shared among several steps in metabolic networks.

5. Conclusion

An interesting advantage of control coefficients with fixed signs is that they confer robustness to the system [14]. Consistently, predictions based on fixed signs of control coefficients are also very robust. The structure of the metabolic network and the regulatory dependences affecting most of the metabolic processes, specifically those associated with the carbon metabolism, are available and sufficient to predict the sign of metabolic control coefficients. We have proposed and verified the use of fixed signs of metabolic control coefficients as a useful tool to evaluate the key enzyme activities underlying metabolic adaptations associated with K-*ras* oncogenic transformation in NIH-3T3 cells. The predicted changes of G6PD, TKT, PK, and LDH activities give very good agreement with the observed pattern of changes in fluxes and concentrations. Thus, with a limited knowledge of the metabolic network structure and regulatory circuits, the proposed analysis arises as a tool which can provide a complete picture of predictable effects based on systemic properties—changes in fluxes and metabolite concentrations—with respect to changes in enzyme activities.

Acknowledgments

We thank Michael John Binns for his careful reading, suggestions and corrections. This study was supported by grants SAF2008-00164, from the Ministerio de Ciencia e Innovación, and from Red Temática de Investigación Cooperativa en Cáncer, Instituto de Salud Carlos III, Spanish Ministry of Science and Innovation & European Regional Development Fund (ERDF) "Una manera de hacer Europa"(ISCIII-RTICC grants RD06/0020/0046). It has also received financial support from the AGAUR-Generalitat de Catalunya (grant 2009SGR1308). PA was supported by a Grant from Generalitat de Catalunya (Programa Beatriu de Pinós). AB was supported by a Grant from Consejo Superior de Investigaciones Científicas (Programa JAE Predoc). RM was supported by a Grant ISCIII: PS09/00965.

References

[1] N. Kozer, G. Schreiber, Effect of crowding on protein–protein association rates: fundamental differences between low and high mass crowding agents, J. Mol. Biol. 336 (2004) 763–774.
[2] T. Ureta, Organización del metabolismo: Localización subcelular de enzimas glicolíticas, Arch. Biol. Med. Exp. 18 (1985) 9–32.
[3] D.A. Fell, Understanding the Control of Metabolism, Portland Press, London, 1997.
[4] A. Cornish-Bowden, Fundamentals of Enzyme Kinetics, third ed., Portland Press, London, 2000.
[5] M. Cascante, L.G. Boros, B. Comin-Anduix, P. de Atauri, J.J. Centelles, P.W. Lee, Metabolic control analysis in drug discovery and disease, Nat. Biotechnol. 20 (2002) 243–249.
[6] D.A. Fell, H.M. Sauro, Metabolic control and its analysis. Additional relationships between elasticities and control coefficients, Eur. J. Biochem. 148 (1985) 555–561.
[7] H.V. Westerhoff, D.B. Kell, Matrix method for determining steps most rate-limiting to metabolic fluxes in biotechnological processes, Biotechnol. Bioeng. 30 (1987) 101–107.
[8] C. Reder, Metabolic control theory: a structural approach, J. Theor. Biol. 135 (1988) 175–201.
[9] M. Cascante, R. Franco, E.I. Canela, Use of implicit methods from general sensitivity theory to develop a systemic approach to metabolic control. I. Unbranched pathways, Math. Biosci. 94 (1989) 271–288.
[10] M. Cascante, R. Franco, E.I. Canela, Use of implicit methods from general sensitivity theory to develop a systemic approach to metabolic control. II. Complex systems, Math. Biosci. 94 (1989) 289–309.
[11] A.K. Sen, Metabolic control analysis. An application of signal flow graphs, Biochem. J. 269 (1990) 141–147.
[12] A.K. Sen, A graph-theoretic analysis of metabolic regulation in linear pathways with multiple feedback loops and branched pathways, Biochim. Biophys. Acta 1059 (1991) 293–311.
[13] A.K. Sen, On the sign pattern of metabolic control coefficients, J. Theor. Biol. 182 (1996) 269–275.
[14] V. Baldazzi, D. Ropers, Y. Markowicz, D. Kahn, J. Geiselmann, H. de Jong, The carbon assimilation network in *Escherichia coli* is densely connected and largely sign-determined by directions of metabolic fluxes, PLoS Comput. Biol. 6 (2010) e1000812.
[15] F. Chiaradonna, D. Gaglio, M. Vanoni, L. Alberghina, Expression of transforming K-Ras oncogene affects mitochondrial function and morphology in mouse fibroblasts, Biochim. Biophys. Acta 1757 (2006) 1338–1356.
[16] F. Chiaradonna, E. Sacco, R. Manzoni, M. Giorgio, M. Vanoni, L. Alberghina, Ras-dependent carbon metabolism and transformation in mouse fibroblasts, Oncogene 25 (2006) 5391–5404.
[17] D. Gaglio, C. Soldati, M. Vanoni, L. Alberghina, F. Chiaradonna, Glutamine deprivation induces abortive s-phase rescued by deoxyribonucleotides in k-ras transformed fibroblasts, PLoS ONE 4 (2009) e4715.
[18] X. Liu, X. Wang, J. Zhang, E.K. Lam, V.Y. Shin, A.S. Cheng, J. Yu, F.K. Chan, J.J. Sung, H. C. Jin, Warburg effect revisited: an epigenetic link between glycolysis and gastric carcinogenesis, Oncogene 29 (2010) 442–450.
[19] M. Malumbres, M. Barbacid, RAS oncogenes: the first 30 years, Nat. Rev. Cancer 3 (2003) 459–465.
[20] K. Rajalingam, R. Schreck, U.R. Rapp, S. Albert, Ras oncogenes and their downstream targets, Biochim. Biophys. Acta 1773 (2007) 1177–1195.
[21] A. Young, J. Lyons, A.L. Miller, V.T. Phan, I.R. Alarcón, F. McCormick, Ras signaling and therapies, Adv. Cancer Res. 102 (2009) 1–17.

[22] S. Guerrero, I. Casanova, L. Farré, A. Mazo, G. Capellà, R. Mangues, K-ras codon 12 mutation induces higher level of resistance to apoptosis and predisposition to anchorage-independent growth than codon 13 mutation or proto-oncogene overexpression, Cancer Res. 60 (2000) 6750–6756.
[23] S. Guerrero, A. Figueras, I. Casanova, L. Farré, B. Lloveras, G. Capellà, M. Trias, R. Mangues, Codon 12 and codon 13 mutations at the K-ras gene induce different soft tissue sarcoma types in nude mice, FASEB J. 16 (2002) 1642–1644.
[24] P. Vizán, L.G. Boros, A. Figueras, G. Capella, R. Mangues, S. Bassilian, S. Lim, W.N. Lee, M. Cascante, K-ras codon-specific mutations produce distinctive metabolic phenotypes in NIH3T3 mice fibroblasts, Cancer Res. 65 (2005) 5512–5515.
[25] S. Wolfram, The Mathematica book, fifth ed., Wolfram Media, Inc, 2003.
[26] A. Kunst, B. Draeger, J. Ziegenhorn, D-Glucose; UV-methods with hexokinase and glucose-6-phosphate dehydrogenase, in: methods of enzymatic analysis, Verlag Chemie, Weinheim, Germany, 1984.
[27] J.V. Passonneau, O.H. Lowry, Enzymatic Analysis: A Practical Guide, The Humana Press Inc., Totowa, New Jersey, USA, 1993.
[28] P. Lund, L-glutamine and L-glutamate; UV-method with glutaminase and glutamate dehydrogenase, in: methods of enzymatic analysis, Verlag Chemie, Weinheim, Germany, 1985.
[29] P. Vizán, G. Alcarraz-Vizán, S. Diaz-Moralli, J.C. Rodríguez-Prados, M. Zanuy, J.J. Centelles, O. Jáuregui, M. Cascante, Quantification of intracellular phosphorylated carbohydrates in HT29 human colon adenocarcinoma cell line using liquid chromatography-electrospray ionization tandem mass spectrometry, Anal. Chem. 79 (2007) 5000–5005.
[30] A. Baracca, F. Chiaradonna, G. Sgarbi, G. Solaini, L. Alberghina, G. Lenaz, Mitochondrial complex I decrease is responsible for bioenergetic dysfunction in K-ras transformed cells, Biochim. Biophys. Acta 1797 (2010) 314–323.
[31] W.N. Tian, L.D. Braunstein, J. Pang, K.M. Stuhlmeier, Q.C. Xi, X. Tian, R.C. Stanton, Importance of glucose-6-phosphate dehydrogenase activity for cell growth, J. Biol. Chem. 273 (1998) 10609–10617.
[32] E.H. Smeets, H. Muller, J. de Wael, A NADH-dependent transketolase assay in erythrocyte hemolysates, Clin. Chim. Acta 33 (1971) 379–386.
[33] W.N. Lee, L.G. Boros, J. Puigjaner, S. Bassilian, S. Lim, M. Cascante, Mass isotopomer study of the nonoxidative pathways of the pentose cycle with [1, 2–^{13}C2]glucose, Am. J. Physiol. 274 (1998) E843–E851.
[34] C.H. Schilling, S. Schuster, B.O. Palsson, R. Heinrich, Metabolic pathway analysis: basic concepts and scientific applications in the post-genomic era, Biotechnol. Prog. 15 (1999) 296–303.
[35] K.J. Kauffman, P. Prakash, J.S. Edwards, Advances in flux balance analysis, Curr. Opin. Biotechnol. 14 (2003) 491–496.
[36] F. Llaneras, J. Picó, Stoichiometric modelling of cell metabolism, J. Biosci. Bioeng. 105 (2008) 1–11.
[37] F. Llaneras, J. Picó, An interval approach for dealing with flux distributions and elementary modes activity patterns, J. Theor. Biol. 246 (2007) 290–308.
[38] H. Pelicano, D.S. Martin, R.H. Xu, P. Huang, Glycolysis inhibition for anticancer treatment, Oncogene 25 (2006) 4633–4646.
[39] H. Nakajima, N. Raben, T. Hamaguchi, T. Yamasaki, Phosphofructokinase deficiency; past, present and future, Curr. Mol. Med. 2 (2002) 197–212.
[40] S. Mazurek, Pyruvate kinase type M2: a key regulator of the metabolic budget system in tumor cells, Int. J. Biochem. Cell Biol. (2010), (doi: 10.1016).
[41] S. Mazurek, H.C. Drexler, J. Troppmair, E. Eigenbrodt, U.R. Rapp, Regulation of pyruvate kinase type M2 by A-Raf: a possible glycolytic stop or go mechanism, Anticancer Res. 27 (2007) 3963–3971.
[42] L. Wang, I. Birol, V. Hatzimanikatis, Metabolic control analysis under uncertainty: framework development and case studies, Biophys. J. 87 (2004) 3750–3763.
[43] G. Kroemer, J. Pouyssegur, Tumor cell metabolism: cancer's Achilles' heel, Cancer Cell 13 (2008) 472–482.
[44] P. Vizán, S. Mazurek, M. Cascante, Robust metabolic adaptation underlying tumor progression, Metabolomics 4 (2008) 1–12.
[45] J.W. Kim, K.I. Zeller, Y. Wang, A.G. Jegga, B.J. Aronow, K.A. O'Donnell, C.V. Dang, Evaluation of myc E-box phylogenetic footprints in glycolytic genes by chromatin immunoprecipitation assays, Mol. Cell. Biol. 24 (2004) 5923–5936.
[46] J.D. Gordan, C.B. Thompson, M.C. Simon, HIF and c-Myc: sibling rivals for control of cancer cell metabolism and proliferation, Cancer Cell 12 (2007) 108–113.
[47] G.L. Semenza, Defining the role of hypoxia-inducible factor 1 in cancer biology and therapeutics, Oncogene 29 (2010) 625–634.
[48] G.L. Semenza, HIF-1: upstream and downstream of cancer metabolism, Curr. Opin. Genet. Dev. 20 (2010) 51–56.
[49] H. Kacser, L. Acerenza, A universal method for achieving increases in metabolite production, Eur. J. Biochem. 216 (1993) 361–367.
[50] W. Kuo, J. Lin, T.K. Tang, Human glucose-6-phosphate dehydrogenase (G6PD) gene transforms NIH 3T3 cells and induces tumors in nude mice, Int. J. Cancer 85 (2000) 857–864.
[51] L.G. Boros, J. Puigjaner, M. Cascante, W.N. Lee, J.L. Brandes, S. Bassilian, F.I. Yusuf, R.D. Williams, P. Muscarella, W.S. Melvin, W.J. Schirmer, Oxythiamine and dehydroepiandrosterone inhibit the nonoxidative synthesis of ribose and tumor cell proliferation, Cancer Res. 57 (1997) 4242–4248.
[52] J. Boren, A.R. Montoya, P. de Atauri, B. Comin-Anduix, A. Cortes, J.J. Centelles, W.M. Frederiks, C.J. Van Noorden, M. Cascante, Metabolic control analysis aimed at the ribose synthesis pathways of tumor cells: a new strategy for antitumor drug development, Mol. Biol. Rep. 29 (2002) 7–12.
[53] B. Comin-Anduix, J. Boren, S. Martinez, C. Moro, J.J. Centelles, R. Trebukhina, N. Petushok, W.N. Lee, L.G. Boros, M. Cascante, The effect of thiamine supplementation on tumour proliferation. A metabolic control analysis study, Eur. J. Biochem. 268 (2001) 4177–4182.
[54] B. Raïs, B. Comin, J. Puigjaner, J.L. Brandes, E. Creppy, D. Saboureau, R. Ennamany, W.-N. Paul Lee, L.G. Boros, M. Cascante, Oxythiamine and dehydroepiandrosterone induce a G1 phase cycle arrest in Ehrlich's tumor cells through inhibition of the pentose cycle, FEBS Lett. 456 (1999) 113–118.
[55] A. Ramos-Montoya, W.N. Lee, S. Bassilian, S. Lim, R.V. Trebukhina, M.V. Kazhyna, C.J. Ciudad, V. Noe, J.J. Centelles, M. Cascante, Pentose phosphate cycle oxidative and nonoxidative balance: a new vulnerable target for overcoming drug resistance in cancer, Int. J. Cancer 119 (2006) 2733–2741.
[56] R. Moreno-Sánchez, E. Saavedra, S. Rodríguez-Enríquez, J.C. Gallardo-Pérez, H. Quezada, H.V. Westerhoff, Metabolic control analysis indicates a change of strategy in the treatment of cancer, Mitochondrion 10 (2010) 626–639, (doi:10.1016).